MCB
Journals.ASM.org

MicroRNA 224 Regulates Ion Transporter Expression in Ameloblasts To Coordinate Enamel Mineralization

Yi Fan,[a,b] Yachuan Zhou,[a,b] Xuedong Zhou,[a,b] Feifei Sun,[a,b] Bo Gao,[a,b] Mian Wan,[a,b] Xin Zhou,[a,b] Jianxun Sun,[a,b] Xin Xu,[a] Lei Cheng,[a] Janet Crane,[c,d] Liwei Zheng[a,b]

State Key Laboratory of Oral Diseases, West China Hospital of Stomatology, Sichuan University, Chengdu, Sichuan, China[a]; West China School of Stomatology, Sichuan University, Chengdu, Sichuan, China[b]; Department of Orthopedics[c] and Department of Pediatrics,[d] School of Medicine, Johns Hopkins University, Baltimore, Maryland, USA

Enamel mineralization is accompanied by the release of protons into the extracellular matrix, which is buffered to regulate the pH value in the local microenvironment. The present study aimed to investigate the role of microRNA 224 (miR-224) as a regulator of *SLC4A4* and *CFTR*, encoding the key buffering ion transporters, in modulating enamel mineralization. miR-224 was significantly downregulated as ameloblasts differentiated, in parallel with upregulation of *SLC4A4* and *CFTR*. Overexpression of miR-224 downregulated *SLC4A4* and *CFTR* expression in cultured human epithelial cells. A microRNA luciferase assay confirmed the specific binding of miR-224 to the 3′ untranslated regions (UTRs) of *SLC4A4* and *CFTR* mRNAs, thereby inhibiting protein translation. miR-224 agomir injection in mouse neonatal incisors resulted in normal enamel length and thickness, but with disturbed organization of the prism structure and deficient crystal growth. Moreover, the enamel Ca/P ratio and microhardness were markedly reduced after miR-224 agomir administration. These results demonstrate that miR-224 plays a pivotal role in fine tuning enamel mineralization by modulating *SLC4A4* and *CFTR* to maintain pH homeostasis and support enamel mineralization.

Tooth enamel is composed of tightly packed hydroxyapatite crystals. As the hardest mineralized tissue in vertebrates, enamel confers protection of masticatory function (1). Similar to other mineralized tissues, enamel is formed through deposition of extracellular matrix (ECM) by secretory ameloblasts (SAB), which is then mineralized by mature ameloblasts (MAB) (2). Both SAB and MAB originate from dental epithelial precursor cells. By sequential differentiation, dental epithelial precursor cells in mice go through several ameloblast lineage cell (ALC) differentiations, including cervical loop (CL) epithelial cells, preameloblasts (PAB), and presecretory ameloblasts (PSAB), and eventually give rise to terminally differentiated ameloblasts, SAB and MAB (Fig. 1A).

Enamel formation is initiated during the secretory stage, when nucleation and crystallite elongation begin, rapidly followed by the maturation stage, when crystallite thickness and width increase. During this process, every unit of hydroxyapatite crystal formation is accompanied by ~8 H^+s released into the extracellular matrix, theoretically resulting in decreased pH in the extracellular space (1). This event continues throughout amelogenesis, peaking in the maturation phase. When measured directly, the pH of the enamel extracellular microenvironment during the secretory stage remains neutral (3). Furthermore, in the later maturation stage, the enamel matrix pH shifts from acidic to neutral, indicating tight modulation of pH homeostasis (1, 4). As previously reported by us and others, ameloblasts play a critical role in regulating pH through various mechanisms, including the buffering system of amelogenin (AMLX) protein (3) and differential ion channel expression in differentiated ameloblasts (5, 6). The ion channels, such as anion exchanger 2 (AE2), electrogenic bicarbonate cotransporter 1 (NBCe1), and cystic fibrosis (CF) conductance transmembrane regulator (CFTR), have been shown to act as a buffering system by modulating the pH during amelogenesis (5, 6). During crystal mineralization, ameloblasts appear as a polarized layer of cells analogous to other bicarbonate-transporting (secretory) epithelia. AE2, encoded by *SLC4A2*, resides at the apical membrane, whereas NBCe1, encoded by *SLC4A4*, resides at the basolateral membrane (5, 6). CFTR, a cyclic-AMP-regulated chloride channel, is located in the apical membranes of polarized ameloblasts.

Several studies have shown that microRNAs (miRNAs) play a key role in epithelial anion transport in bicarbonate-transporting (secretory) epithelia to spatially and temporally regulate expression. miRNAs function posttranscriptionally by binding the 3′ untranslated region (UTRs) of mRNAs and suppressing their translation, ultimately leading to mRNA degradation (7). miRNAs play a role in almost all aspects of metazoan biology by buffering cell states, as well as driving cell fate transitions (8). CFTR has been reported to be regulated by microRNA 138 (miR-138) in airway epithelia through interaction with the transcriptional regulatory protein SIN3A (9). AE2 activity is diminished by miR-506 upregulation in cholangiocytes from primary biliary cirrhosis patients, which binds directly to the 3′ UTR region of *Slc4a2* mRNA, ultimately impairing

Received 15 October 2014 **Returned for modification** 15 November 2014
Accepted 4 June 2015

Accepted manuscript posted online 8 June 2015

Citation Fan Y, Zhou Y, Zhou X, Sun F, Gao B, Wan M, Zhou X, Sun J, Xu X, Cheng L, Crane J, Zheng L. 2015. MicroRNA 224 regulates ion transporter expression in ameloblasts to coordinate enamel mineralization. Mol Cell Biol 35:2875–2890. doi:10.1128/MCB.01266-14.

Address correspondence to Liwei Zheng, zhenglw399@hotmail.com.

Y.F. and Y.Z. contributed equally to this article.

doi:10.1128/MCB.01266-14

The authors have paid a fee to allow immediate free access to this article.

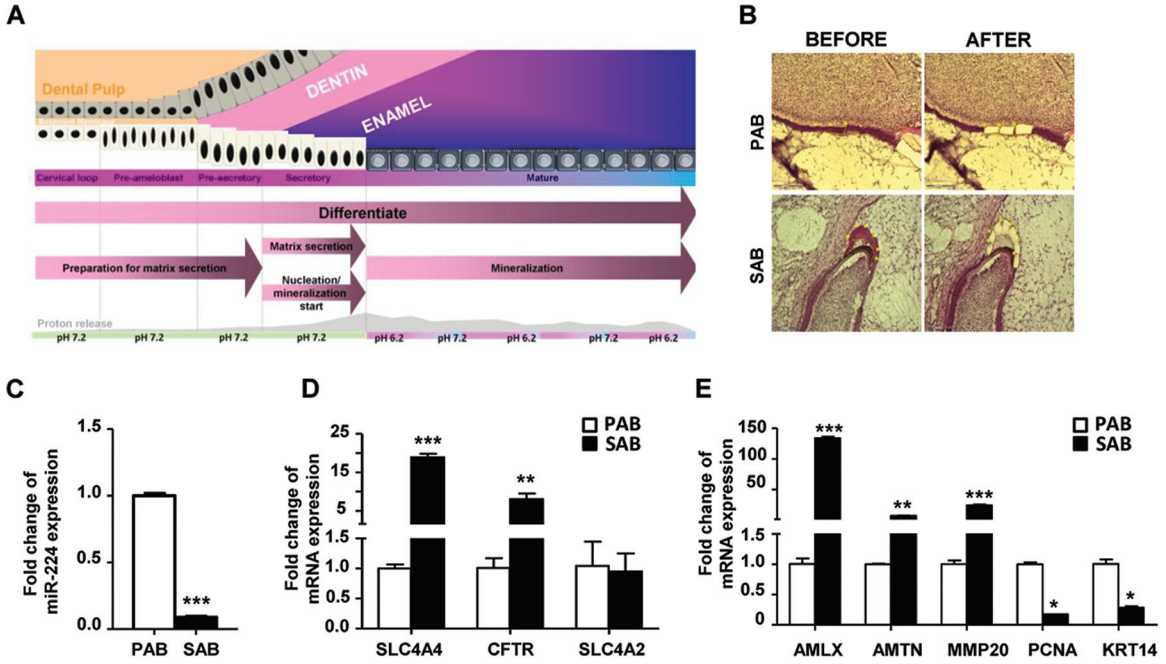

FIG 1 Characterization of ameloblast differentiation in human tooth buds by LCM. (A) Schematic illustration of ameloblast differentiation and enamel formation. (B) Preameloblasts and secretory ameloblasts from human fetal tooth buds were collected by LCM. BEFORE, before dissection; AFTER, after dissection. (C) miR-224 mRNA expression levels in PAB and SAB. (D) *SLC4A4*, *CFTR*, and *SLC4A2* mRNA expression levels in PAB and SAB were determined by qRT-PCR. (E) Enamel formation-associated gene (*AMLX*, *AMTN*, *MMP20*, *PCNA*, and *KRT14*) expression levels in PAB and SAB were determined by qRT-PCR. *, $P < 0.05$; **, $P < 0.01$; ***, $P < 0.001$ (comparison between PAB and SAB; $n = 5$). The data are represented as means and standard deviations (SD).

biliary secretory functions (10). In the current study, we sought to investigate whether miRNAs are also involved in ameloblast differentiation and enamel mineralization through regulation of ion transporter expression in ameloblasts. In our previous study, we determined by miRNA microarray that miR-224 levels differ significantly between early and late bell stages of the human tooth germ (11). Prediction tools (TargetScan and miRBase) indicated miR-224 as a candidate to target *SLC4A4* and *CFTR* mRNAs. We therefore aimed to investigate the potential role of miR-224 as a regulator of ameloblast differentiation and enamel mineralization.

MATERIALS AND METHODS

Ethics statement and tissue samples. The study and collection of human or mouse samples was approved by the Ethical Committees of the West China School of Stomatology, Sichuan University, and the State Key Laboratory of Oral Diseases. All human tissues were acquired from the West China Women and Children's Hospital according to guidelines approved by Sichuan University. For use of the tissue samples, written informed consent of all human subjects who participated in the experiment was obtained. Human tooth buds and buccal epithelium were collected from 15- to 25-week-old fetal cadavers within 3 h after legal abortion. The mandibles, including the tooth buds, were dissected under a laminar flow hood and embedded in OCT compound (Surgipath; Leica, USA) for laser capture microdissection (LCM).

LCM. Human tissue samples containing tooth buds were cut into 10-μm sections and then applied to PEN membrane glass slides (Arcturus). LCM was performed with an Arcturus XT laser capture microdissection system using CapSure Macro Caps (Arcturus). Epithelial cells from PAB and SAB were separately isolated by LCM (Fig. 1B). PAB were the polarized inner enamel epithelial cells that were in direct contact with the basement membrane and adjacent to polarized odontoblasts. SAB were identified as polarized epithelial cells in direct contact with the enamel matrix. Approximately 10,000 cells were captured on each of 10 caps per sample. Total RNA, including small RNAs, was extracted from captured cells using an miRNeasy minikit (Qiagen Inc., Valencia, CA) according to the manufacturer's instructions.

Cell culture. Human fetal oral buccal mucosal epithelial cells (OEs) and ALCs were cultured as described previously (12) in KGM-2 medium (Lonza, Basel, Switzerland) with 1% penicillin/streptomycin, and 0.05 mmol/liter calcium on BD Primaria tissue culture dishes (BD Biosciences, Franklin Lakes, NJ). Clonally selected cells were grown at either pH 7.2 with 0, 10, and 50 μM fluoride or at pH 6.2 without fluoride for 72 h.

Oligonucleotide transfection. The miR-224 mimic (product identifier [ID], miR10000281), miR-224 mimic negative control (NC) (product ID, miR01101), miR-224 inhibitor (product ID, miR20000281), miR-224 inhibitor negative control (product ID, miR02101), miR-130a mimic (product ID, miR10000425), miR-330 mimic (product ID, miR10000751), and miR-188 mimic (product ID, miR10000457) were synthesized by Ribobio (Guangzhou, China). miRNA mimics are chemically synthesized double-stranded small RNAs that mimic the endogenous miRNA function and regulate the corresponding target genes by using endogenous miRNA machinery. The sequences of the miRNA mimics were as follows: miR-224 mimic, 5′-CAAGUCACUAGUGGUUCCGUU-3′ and 3′-AACGGAACCACU AGUGACUUG-5′; miR-130a mimic, 5′-CAGUGCAAUGUUAAAAG GGCAU-3′ and 3′-GUCACGUUACAAUUUUCCCGUA-5′; miR-330 mimic, 5′-GCAAAGCACACGGCCUGCAGAGA-3′ and 3′-CGUUUC GUGUGCCGGACGUCUCU-5′; and miR-188 mimic, 5′-CAUCCCU UGCAUGGUGGAGGG-3′ and 3′-GUAGGGAACGUACCACCUCC C-5′. miR-224 inhibitors are chemically synthesized single-stranded RNA molecules with unique sequence that may bind to and hence inhibit miRNAs. The sequence of miR-224 inhibitors was 5′-AACGG AACCACUAGUGACUUG-3′. Oligonucleotide transfection was carried out using Lipofectamine 2000 reagents (Life Technology). The final concentrations of the miR-224 mimic and miR-224 inhibitor in the transfection system were 50 nM and 200 nM, respectively. The concentration of the miR-130a mimic, miR-330 mimic, and miR-188

mimic was 50 nM. The miRNA mimic NC and inhibitor NC served as controls and showed minimal homology to all known miRNAs to eliminate off-target effects.

RNA extraction and qRT-PCR. Total RNA, including small RNAs from cells, was isolated with an miRNeasy minikit (Qiagen). The RNA concentration was determined with a NanoDrop ND-1000 (Thermo Fisher Scientific). miR-224, miR-130a, miR-330, and miR-188 reverse transcription (RT) was performed with the TaqMan microRNA reverse transcription kit using specific RT primers according to the manufacturer's instructions. The quantitative real-time RT-PCR (qRT-PCR) for miR-224, miR-130a, miR-330, and miR-188 was performed with the TaqMan Small RNA assay. cDNA synthesis for mRNA was performed using the SuperScript first-strand synthesis system (Life Technology). The mRNA levels of genes were subjected to qRT-PCR with PowerSYBR Green PCR master mix and an ABI 7900 system (Applied Biosystems). Relative gene expression levels were normalized by U6 or GAPDH (glyceraldehyde-3-phosphate dehydrogenase) using the $\Delta\Delta C_T$ method.

Western blotting. After oligonucleotide transfection, total cellular protein was extracted using a reagent kit (KeyGEN, Nanjing, Jiangsu, China), and bicinchoninic acid (BCA) protein assays were used to determine protein concentrations (Beyotime, Haimen, Jiangsu, China). An equal amount of each sample (20 μg) was electrophoresed on SDS-PAGE and then transferred to a nitrocellulose membrane. After blocking, the membranes were incubated with primary antibody: goat anti-NBCe1 (C-14; 1:200), rabbit anti-CFTR (H-182; 1:200), goat anti-AE2 (1:200), goat anti-K14 (C-14; 1:500), rabbit antiamelogenin (FL-191; 1:100), goat antiameloblastin (AMBN) (N-18; 1:100), or mouse anti-GAPDH (D-6; 1:500) (Santa Cruz Biotechnology). The membranes were then incubated with goat anti-rabbit IgG–horseradish peroxidase (HRP), rabbit anti-goat IgG-HRP, or goat anti-mouse IgG-HRP (Santa Cruz Biotechnology) and detected with a chemiluminescent reagent kit (Millipore). GAPDH expression served as an internal control. For image analysis, the film was scanned and analyzed with a GS-700 imaging densitometer (Bio-Rad).

Luciferase assay. For functional analysis of miR-224, we designed oligonucleotide pairs of the mRNA 3′ UTR containing the miR-224 binding sequences for *SLC4A4* and *CFTR* oligonucleotides as mutation groups. The pmirGLO vector was linearized with PmeI and XbaI restriction enzymes (New England BioLabs) to generate overhangs complementary to the annealed oligonucleotide overhangs. Then, the oligonucleotides were combined with oligonucleotide-annealing buffer (Promega) and heated at 90°C for 3 min, followed by 15 min in a 37°C water bath. The annealed oligonucleotides were diluted 1:10 to a final concentration of 4 ng/μl per oligonucleotide. A 4-ng quantity of annealed oligonucleotides was ligated with 50 ng of linearized vector. Ligated pmirGLO vector was then transformed with high-efficiency JM109 competent cells. Ampicillin-containing plates were used to select clones, which were then digested with the QIAprep Spin MiniPrep kit (Qiagen). The correct orientation of the 3′ UTR fragments in the plasmid DNA constructs was confirmed by sequencing analysis. The double-stranded miR-224 mimics and mimic NC were synthesized by Ribobio (Guangzhou, China). The concentrations of miR-224 mimics and mimic NC plasmids in the transfection system were 50 nM and 200 nM, respectively. Transient transfection of HEK-293T cells was performed in 96-well plates according to the manufacturer's instructions with Lipofectamine 2000 (Invitrogen). Twenty-four hours after transfection, luciferase activity was determined with a Dual-Glo luciferase assay system (Promega) and a MicroLumatPlus LB96V luminometer (Berthold Technologies). Normalized firefly luciferase activity and *Renilla* luciferase activity for each construct were compared with a pmirGLO vector no-insert control. For each transfection, the luciferase activity was averaged from three replicates.

***In vivo* assay.** The animal protocols were reviewed and approved by the West China School of Stomatology, Sichuan University. Experiments were carried out in accordance with guidelines established by the National Institutes of Health (NIH) regarding the care and use of animals for experimental procedures. miR-224 agomir (product ID, miR40000671), miR-224 agomir NC (product ID, miR04201), miR-130a agomir (product ID, miR40016983-1-10), miR-330 agomir (product ID, miR40000569), and miR-188 agomir (product ID, miR40000217) were synthesized by Ribobio. These miR agomirs were optimized versions of target miRNA mimics, which upregulate the endogenous miRNA activity by utilizing the natural miRNA machinery. They exhibit enhanced cellular uptake, stability, and regulatory activity *in vivo*. The miR-224 agomir NC was designed for minimum homology to miRNAs. All agomirs and agomir NCs were diluted with sterile phosphate-buffered saline (PBS) to a final concentration of 0.1 nmol/μl. For single injections, 10 μl miR-224 agomir (0.1 nmol/μl), miR-224 agomir NC, and PBS were injected on the lingual side of the cervical loop area. At 0, 24, and 72 h after injection, the mice were sacrificed by decapitation, and the incisor tooth germ was dissected for further microRNA isolation. Based on miR-224 expression levels, 10 μl miR-224 agomir, miR-224 agomir NC, miR-130a agomir, miR-330 agomir, and miR-188 agomir (0.1 nmol/μl) were injected on postnatal day 6 (P6), P9, P12, P15, P18, P21, P24, P27, and P30 on the lingual side of the cervical loop area. The animals of the vehicle group were injected with an equal amount of PBS, and noninjected mice were used as an untreated control group. Each experimental group consisted of 6 mice.

Histology and immunofluorescence. The left mandibles of all seven groups were dissected out and fixed in 4% paraformaldehyde (PFA). After decalcification, the samples were processed and embedded in paraffin. Four-micrometer-thick were cut using a microtome (model HM 340E; Microm, Germany). Standard hematoxylin and eosin (H&E) staining was used to examine tissue histology. The primary antibodies goat anti-NBCe1 (C-14; 1:200), rabbit anti-CFTR (H-182; 1:200), goat anti-AE2 (1:200), and rabbit anti-collagen type I (1:100) (Rockland) were incubated overnight at 4°C and detected with fluorescein-conjugated AffiniPure mouse anti-goat IgG(H+L) (1:100) and tetramethyl rhodamine isothiocyanate (TRITC)-conjugated AffiniPure goat anti-rabbit IgG(H+L) (1:200) for 1 h at room temperature. DAPI (4′,6-diamidino-2-phenylindole) was used for counterstaining. After mounting, the slides were photographed with a Nikon Eclipse 300 fluorescence microscope (Compix Inc., Sewickley, PA).

Micro-CT. Samples were imaged on a micro-computed-tomography (micro-CT) scanner (VivaCT40; SCANO, Switzerland). The right-side mandible was scanned to obtain sagittal sections at a 10.5-μm voxel size, applying an electrical potential of 70 kV_p (where V_p is peak voltage) and 114 μA. Three-dimensional (3D) models were reconstructed using a global threshold that included enamel, dentin, and bone structures. Coronal sections were taken from the mesial, bifurcate, and distal root of first molars and the mesial apex of second molars. The total enamel length was measured with sagittal images.

SEM analysis and SEM-EDX spectroscopy. For scanning electron microscopy (SEM) analysis, the right lower incisors were dissected out and ground in the sagittal direction using 2,500-grit waterproof silicon carbide paper. After grinding and water brushing, the incisors were etched for 45 s in 1% nitric acid and sputtered with gold before observation with a scanning electron microscope (Quanta 400 FEG; FEI/Oxford Instruments/HKL, Eindhoven, Netherlands) at 20 kV. Moreover, the enamel Ca/P mass ratio was verified via energy-dispersive X-ray (EDX) using SEM. The specimens were prepared as described above. Five points in each incisal and cervical enamel region were randomly selected and analyzed by SEM-EDX spectroscopy (WinEDX 3 software). The distributions and atomic concentrations of Ca and P in the tissue were examined, and the Ca/P ratio was calculated.

Vickers microhardness test. The extracted mandibular incisors from miR-224 agomir-treated mice and the other six control groups were washed and embedded sagittally in hard-formulation epoxy resin (see Fig. 10A). Samples were then ground using 2,500-grit waterproof silicon carbide paper and polished to 0.25 mm with diamond suspensions. The polished samples were measured using a Vickers diamond indenter in a

microhardness test machine (Matsuzawa/MMT-X) with 25-g loading for 5 s. At least five indentations per sample in both incisal and cervical areas of the enamel were performed.

Statistical analysis. All experiments were performed independently at least three times in triplicate. Statistical significance was evaluated by Student's *t* test or by one-way analysis of variance (ANOVA), followed by Tukey's test. Bands from Western blotting were quantified with Image Lab software (Bio-Rad). *P* values of <0.05 were considered statistically significant.

RESULTS

miR-224 downregulation paralleled ameloblast differentiation in developing human tooth germ. Cell differentiation and matrix secretion peak between the early and late bell stages in tooth germs. In our previous study (11), microarray results indicated that miR-224 expression significantly decreased in the late bell stage compared to the early bell stage in the human tooth germ. In the present study, this was further confirmed in human developing incisors using laser-captured, microdissected PAB and SAB. miR-224 was statistically downregulated as ameloblasts differentiated from PAB to SAB (Fig. 1C, PAB versus SAB; $P < 0.001$; $n = 5$). Thereafter, miR-224 downregulation in the human enamel organ paralleled ameloblast differentiation.

***SLC4A4* and *CFTR* upregulation paralleled ameloblast differentiation in developing human tooth germ.** NBCe1 has previously been shown to be upregulated in human ameloblasts as cells differentiate and matrix forms (6). To further investigate ion transporter regulation in ameloblasts, qRT-PCR analysis was performed on microdissected ameloblasts from human tooth buds. *SLC4A4* and *CFTR* mRNAs, putative targets of miR-224, were both significantly increased in SAB compared to PAB (Fig. 1D). *SLC4A2* mRNA expression levels remained unchanged. During the secretory stage, ameloblasts start secreting large amounts of enamel matrix proteins into the enamel matrix (2). The genes known to be involved in amelogenesis, including *AMLX*, *AMTN*, and *MMP20*, were significantly upregulated in SAB compared to PAB, while *PCNA* and *KRT14* were further decreased as dental epithelial cells differentiated into ameloblasts (Fig. 1E), which, on the other hand, demonstrated the accurate identification of PAB and SAB from which samples were dissected.

miR-224 regulated *SLC4A4* and *CFTR* expression in cultured human epithelial cells. Human fetal OEs and ALCs were cultured in order to investigate the function of miR-224 in human epithelial cells *in vitro*. OEs and ALCs are derived from the same progenitor cell source, but OE is not secretory epithelium (12). In the present study, the miR-224 mimic and inhibitor were transfected into either cultured ALCs or OEs. The efficiency of transfection was validated by qRT-PCR. In cultured ALCs and OEs, the miR-224 level was robustly increased after miR-224 mimic transfection and downregulated after miR-224 inhibitor transfection compared to miR-224 mimic NC and miR-224 inhibitor NC transfection, respectively (Fig. 2A and G). The mRNA expression levels of *SLC4A4*, *CFTR*, and *SLC4A2* were significantly decreased 72 h after miR-224 mimic transfection (Fig. 2B and H). In contrast, when transfected with miR-224 inhibitors, mRNA levels of *SLC4A4* and *CFTR* were upregulated, while no change was detected in *SLC4A2* expression (Fig. 2C and I). The expression level of *K14* remained the same (Fig. 2B, C, H, and I). These findings were corroborated by Western blot analysis, which revealed decreased NBCe1 and CFTR protein concentrations after miR-224 mimic transfection and, conversely, upregulation after miR-224 inhibitor transfection in cultured human ALCs (Fig. 2D to F). In human OEs, miR-224 mimic and inhibitor transfection resulted in the same readout (Fig. 2J to L). Although the *SLC4A2* mRNA expression level was downregulated after miR-224 mimic transfection, the AE2 protein concentration was not affected (Fig. 2B, D, H, and J). The K14 protein level also remained unchanged after miR-224 mimic and inhibitor transfection (Fig. 2B to F and H to L).

We had previously obtained miRNA expression profiles from developing human tooth germ, which revealed abundant miRNA expression patterns (11). From this database, we selected three miRNAs (i.e., miR-130a, miR-330, and miR-188) as miRNA controls to assess the specificity of miR-224 function in *SLC4A4* and *CFTR* expression. From our microarray data (11), miR-130a and miR-330 have been shown to have significantly different expression levels from the early to the late bell stage, whereas miR-188 remained unchanged. Several independent studies have identified miR-130a as one of the antiangiogenic miRNAs involved in angiogenesis and vascular development (13, 14). Thus far, there had been no findings regarding the functional roles of miR-330 and miR-188 in regulating epithelium or tooth development. Therefore, we performed miR-130a, miR-330, and miR-188 mimic transfections in human ALCs to determine their roles regarding ion transporters in ameloblasts. qRT-PCR analysis revealed markedly elevated expression levels of miR-130a, miR-330, and miR-188 after each miRNA mimic transfection, suggesting efficient transfection (Fig. 3A). We then analyzed miR-224 expression after miR-130a, miR-330, and miR-188 mimic transfection and found no subsequent changes in miR-224. Significant elevation could be observed only after miR-224 mimic transfection (Fig. 3B). In addition, miR-224 mimic transfection had no effect on miR-130a, miR-330, and miR-188 (Fig. 3C), indicating no cross effect among selected miRNAs. To investigate whether there is alteration in ion transporter expression in response to miR-130a, miR-330, and miR-188, qRT-PCR and Western blotting were performed. No changes in *SLC4A4*, *CFTR*, and *SLC4A2* could be observed in cells subjected to miR-130a, miR-330, and miR-188 mimic transfection, while the miR-224 mimic specifically reduced target gene expression. *K14* remained the same among all groups (Fig. 3D). Western blotting further confirmed the mRNA data. No changes were found in NBCe1, CFTR, AE2, or K14 protein expression levels after miR-130a, miR-330, or miR-188 mimic transfection, while overexpression of miR-224 significantly downregulated NBCe1 and CFTR (Fig. 3E to H), indicating the specific role of miR-224 in mediating *SLC4A4* and *CFTR* expression levels.

During the secretory stage of amelogenesis, ameloblasts secrete different proteins into the enamel extracellular matrix, including AMLX and AMBN, which comprise about 95% to 97% of the organic matrix in the secretory stage (15). Therefore, we investigated the expression levels of AMLX and AMBN after miR-224 mimic and inhibitor transfection. In human ALCs, miR-224 mimic and miR-224 inhibitor transfection had no significant effect on AMLX and AMBN expression levels at both the mRNA and protein levels (Fig. 4A to C). Linear correlation analysis showed that miR-224 expression was linearly and inversely correlated with *SLC4A4* and *CFTR* expression in cultured human ALCs. The correlation coefficients ($R^2 = 0.697$ and 0.737, respectively) had statistical significance ($P < 0.05$). However, *SLC4A2* and *AMLX* had

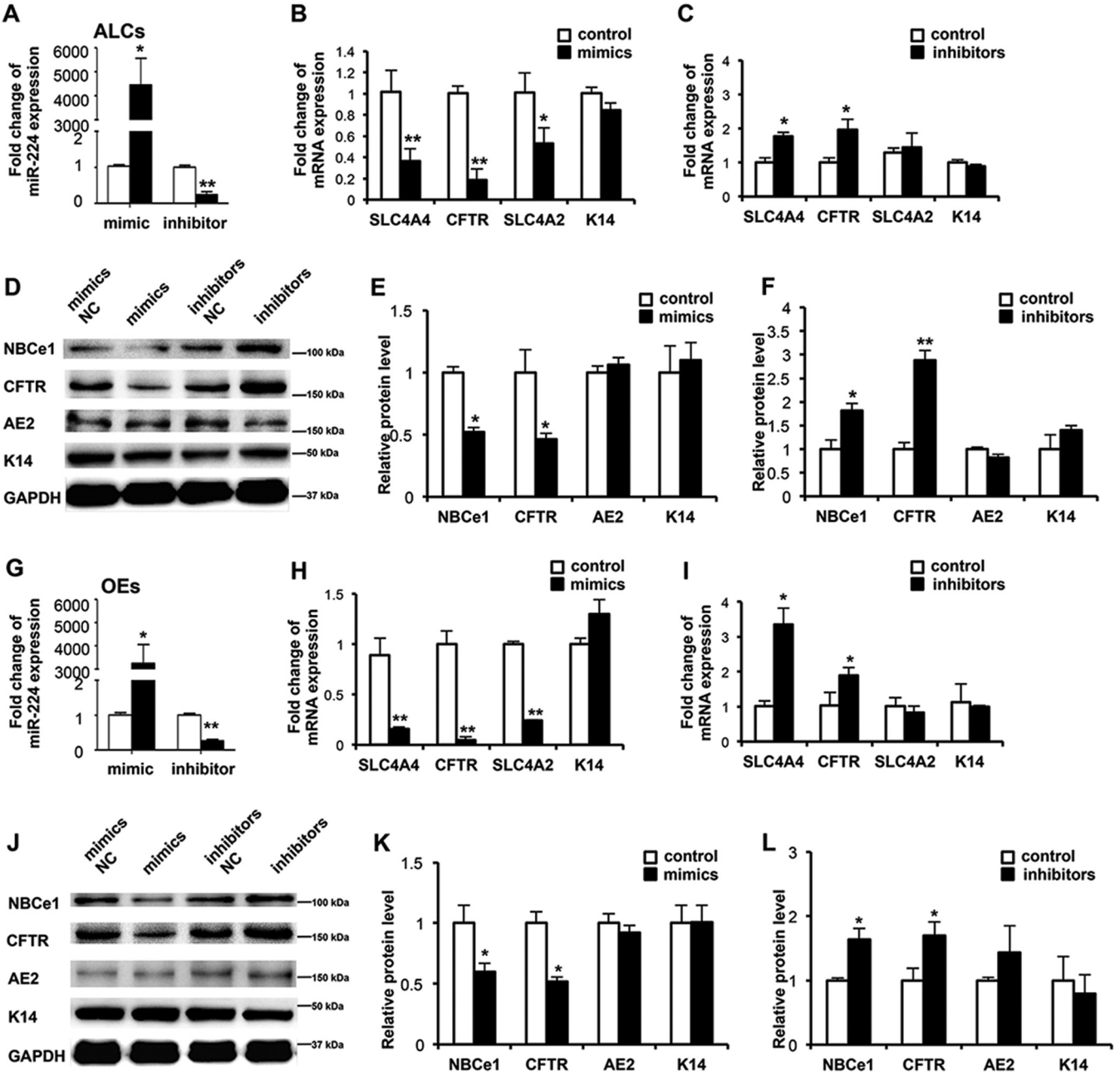

FIG 2 miR-224 regulates *SLC4A4* and *CFTR* expression in cultured human fetal ALCs and OEs. (A and G) miR-224 expression was upregulated after miR-224 mimic transfection and downregulated after miR-224 inhibitor transfection in ALCs (A) and in OEs (G). (B and H) mRNA expression levels of *SLC4A4*, *CFTR*, *SLC4A2*, and *K14* after miR-224 mimic transfection in ALCs (B) and OEs (H). (C and I) mRNA expression levels of *SLC4A4*, *CFTR*, *SLC4A2*, and *K14* after miR-224 inhibitor transfection in ALCs (C) and OEs (I). (D to F and J to L) Western blots showing that the protein levels of NBCe1 and CFTR were downregulated in ALCs (D to F) and OEs (J to L) after miR-224 mimic transfection and were upregulated after miR-224 inhibitor transfection. The protein levels of AE2 and K14 remained the same. *, $P < 0.05$; **, $P < 0.01$ (comparison between control and after treatment; $n = 6$). The data are represented as means and SD.

no correlative relationship with miR-224 expression ($R^2 = 0.482$, $P > 0.05$, and $R^2 = 0.246$, $P > 0.05$, respectively) (Fig. 4D).

miR-224 directly binds to the 3′ UTRs of *SLC4A4* and *CFTR* mRNAs. TargetScan and miRBase indicated that the 3′ UTRs of *SLC4A4* and *CFTR* were putative targets of miR-224. To validate a direct interaction between these candidate genes, we first located the seed sequences for miR-224 in the 3′ UTRs of *SLC4A4* and *CFTR*. The oligonucleotide was synthesized and then cloned into the luciferase reporter vector pmirGLO and cotransfected with the miR-224 or a scrambled microRNA negative control in HEK-293T cells. A dual-luciferase assay revealed that the miR-224 mimic effectively suppressed luciferase reporter activities at those sites. Moreover, mutations significantly impaired the activity of miR-224, relieving repression of luciferase activity (Fig. 4E and F). These data indicated that miR-224 directly binds to the 3′ UTRs of *SLC4A4* and *CFTR*,

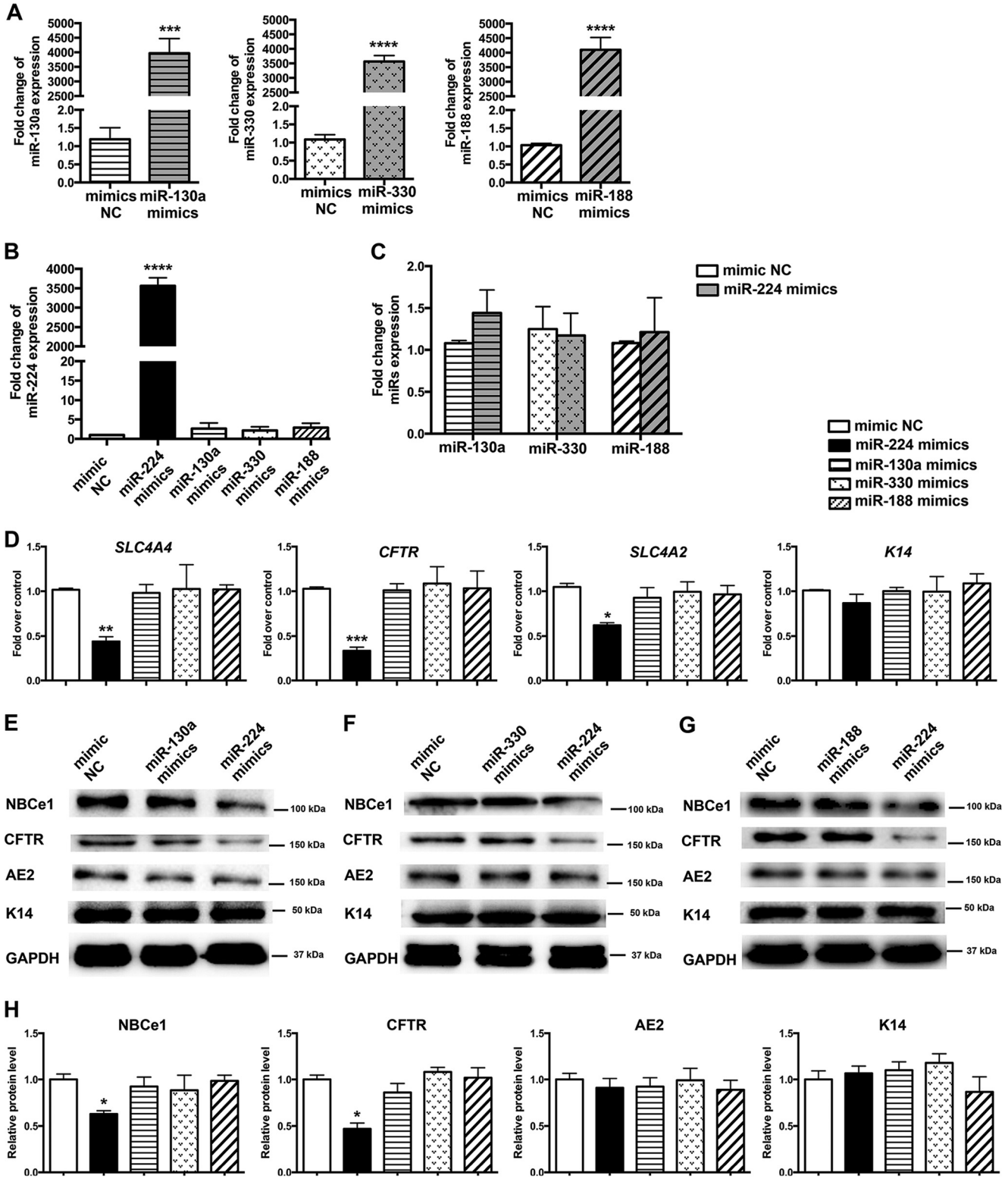

FIG 3 Multiple control miRNAs (miR-130a, miR-330, and miR-188) had no impact on *SLC4A4* and *CFTR* expression in cultured human ALCs. (A) miR-130a, miR-330, and miR-188 expression was markedly increased after miR-130a, miR-330, and miR-188 mimic transfection, respectively. (B) No change was observed in miR-224 expression after miR-130a, miR-330, and miR-188 mimic transfection compared to controls, whereas the miR-224 mimic specifically upregulated miR-224. (C) There were no subsequent alterations in miR-130a, miR-330, or miR-188 after miR-224 mimic administration. (D) qRT-PCR results showed unchanged *SLC4A4*, *CFTR*, *SLC4A2*, and *K14* expression levels after miR-130a, miR-330, and miR-188 mimic treatment. (E to H) Western blotting further indicated no significant alterations of NBCe1, CFTR, SLC4A2, or K14 protein levels. The statistically decreased levels of SLC4A4 and CFTR can be observed only by miR-224 mimic transfection (D to H). *, $P < 0.05$; **, $P < 0.01$; ***, $P < 0.001$; ****, $P < 0.0001$; $n = 4$ to 6. The data are represented as means and SD.

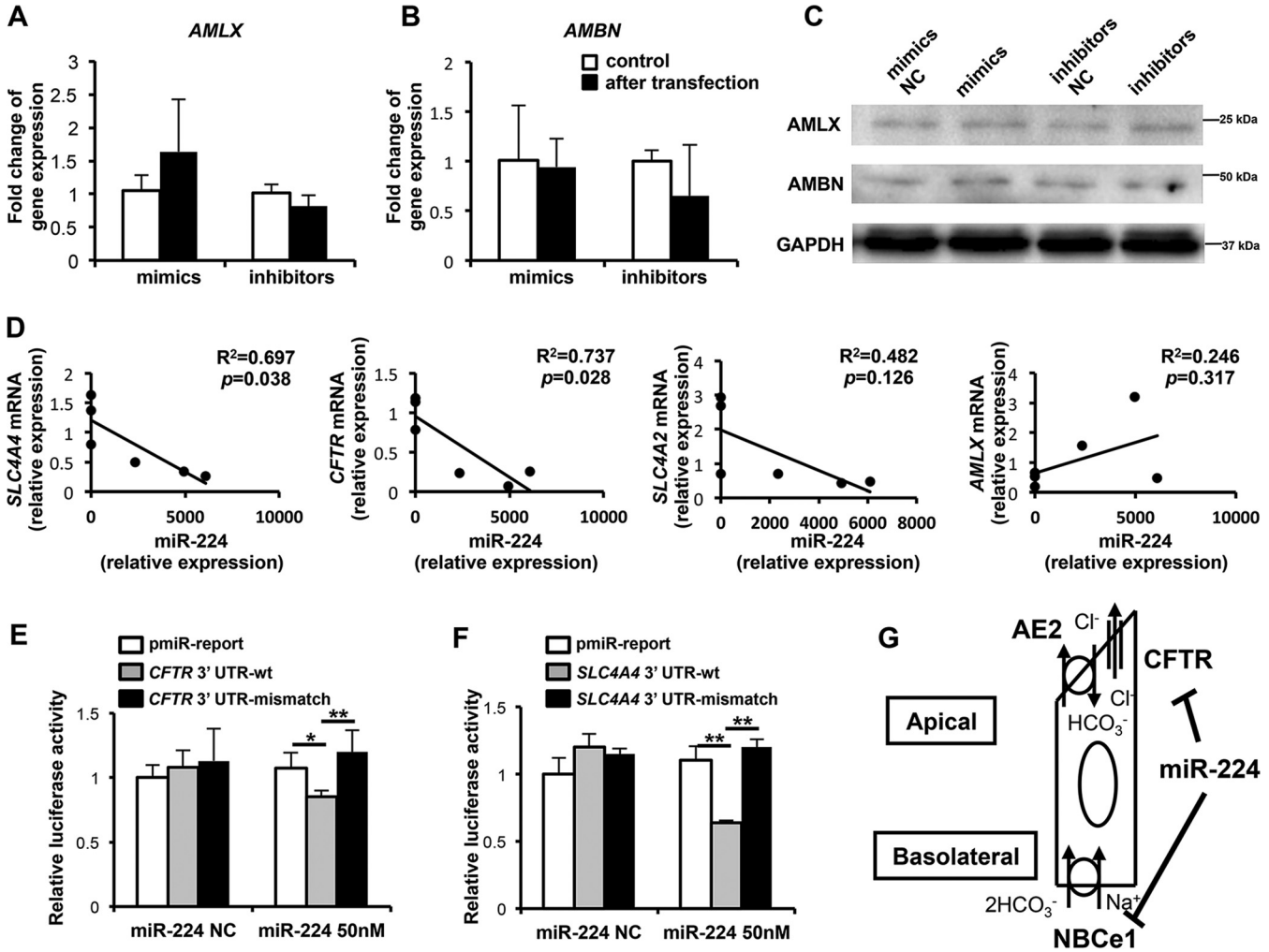

FIG 4 miR-224 directly binds to the 3′ UTRs of *SLC4A4* and *CFTR* mRNAs, with no impact on enamel matrix protein expression. (A and B) qRT-PCR analysis showed unchanged amelogenin (*AMLX*) and ameloblastin (*AMBN*) gene expression levels after miR-224 mimic or miR-224 inhibitor transfection. (C) Unaltered AMLX and AMBN protein levels after miR-224 mimic and miR-224 inhibitor transfection by Western blotting. (D) Linear correlation analyses showed that miR-224 expression is inversely correlated with *SLC4A4* and *CFTR* mRNA expression levels in *in vitro*-cultured human ALCs, whereas *SLC4A2* and *AMLX* had no correlation with miR-224 expression. (E and F) Dual-luciferase assay results indicated that miR-224 acts directly on the 3′ UTRs of *CFTR* and *SLC4A4* mRNAs. (G) Schematic illustration of miR-224 direct activity on and posttranscriptional regulation of *SLC4A4* and *CFTR* on ameloblasts. *, $P < 0.05$; **, $P < 0.01$; $n = 6$. The data are represented as means and SD.

thereby posttranscriptionally modulating these genes (Fig. 4G).

Acidification and fluoride treatment of human ALCs. NBCe1 and CFTR have been proposed to function as a buffering system in ameloblasts and to regulate pH values in the local microenvironment (6). Acidification (pH 6.2 for 72 h) treatment of *in vitro*-cultured human ALCs markedly downregulated miR-224 expression (Fig. 5A) and, in comparison, upregulated *SLC4A4* and *CFTR* expression levels (Fig. 5B). Fluorosis is caused by excessive fluoride intake during enamel development and results in an enamel defect due to a decreased local pH value of the ECM microenvironment (16). We previously reported that fluoride ingestion stimulated *Slc4a4* mRNA in maturation ameloblasts *in vivo*, but there was no effect of fluoride *in vitro*, suggesting fluoride indirectly regulates *Slc4a4* in mice (6). In the current study, fluoride exposure (up to 50 μM) had no significant effect on miR-224, *SLC4A4*, *CFTR*, or *SLC4A2* in human ALCs (Fig. 5C, D, and E). In addition, *AMLX* expression was markedly upregulated in response to acidification but not statistically altered with fluoride treatment (Fig. 5B, D, and E).

miR-224 disrupted ameloblast organization and affected NBCe1 and CFTR expression in developing mouse incisors. To investigate the role of miR-224 in regulating ion transporters of ameloblasts and its role in enamel mineralization *in vivo*, neonatal mice were injected with miR-224 agomir, miR-224 agomir NC, miR-130a agomir, miR-330 agomir, miR-188 agomir, or vehicle (PBS). Noninjected mice were also included as one of the controls. We first evaluated the expression levels of miR-224 at 0 h, 24 h, and 72 h after single injections. miR-224 agomir injection effectively increased miR-224 levels compared to miR-224 agomir NC- and vehicle-injected and noninjected incisors, suggesting specific miR-224 elevation by miR-224 agomir injection. In addition, after miR-224 agomir treatment, the significantly increased level of miR-224 descended to the normal range after 72 h (Fig. 6A). Based

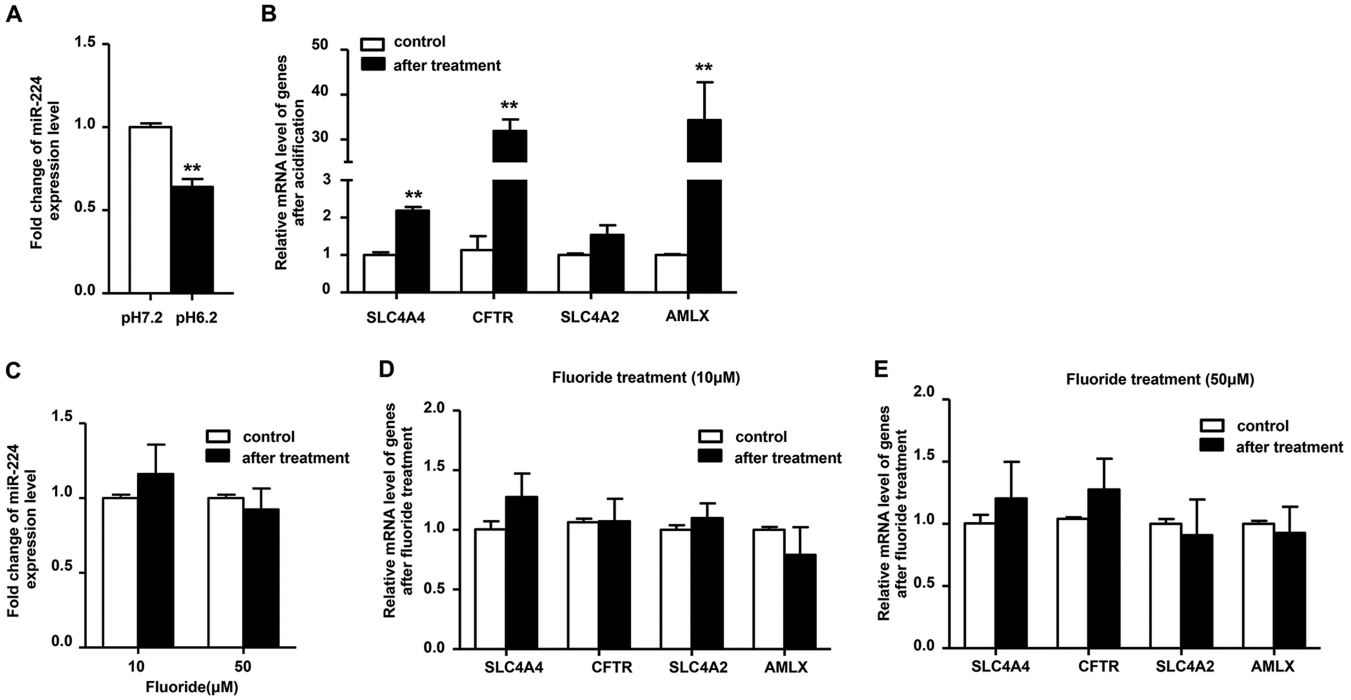

FIG 5 Acidification and fluoride treatment of cultured human ALCs. (A) Human fetal ALCs cultured at low pH (pH 6.2) showed significantly downregulated miR-224 expression. (B) *SLC4A4*, *CFTR*, and *AMLX* mRNA expression levels were significantly upregulated in ALCs cultured under acidification (pH 6.2) for 72 h. (C) Fluoride exposure (10 μM and 50 μM) had no effect on the miR-224 expression level. (D and E) *SLC4A4*, *CFTR*, *SLC4A2*, and *AMLX* showed no significant change after fluoride treatment at 10 μM and 50 μM. **, $P < 0.01$ (comparison between control and after treatment; $n = 6$). The data are represented as means and SD.

on these results, we performed injections every 4 days from P6 to P30 (P6, P9, P12, P15, P18, P21, P24, P27, and P30). At P30, mandibular incisors of miR-224 agomir-, miR-224 agomir NC-, miR-130a agomir-, miR-330 agomir-, miR-188 agomir-, and vehicle-injected mice and noninjected control mice all erupted correctly (Fig. 6B). Histological analysis by H&E staining revealed correctly formed dental epithelial sheets in all seven groups (Fig. 6C to I). However, morphological irregularities were detected in ameloblasts of miR-224 agomir-injected incisors compared to multiple control mice. The dental epithelial cells of miR-224 agomir NC-, miR-130a agomir-, miR-330 agomir-, miR-188 agomir-, and vehicle-injected and control mice at the SAB (Fig. 6D1 to I1), the PAB (Fig. 6D2 to I2), and the CL (Fig. 6D3 to I3) exhibited normal cellular morphology. The ameloblasts were in very intimate contact with each other. These cells were elongated, with nuclei shifted distally toward the stratum intermedium, although the cells in the cervical loop in the miR-224 agomir-treated group (Fig. 6C3) appeared to be in a well-arranged cell layer at the outer CL sheet compared to the arrangement of the CL cells of the other six groups (Fig. 6D3 to I3). The ameloblasts in the SAB and PAB regions of miR-224 agomir-treated mice revealed irregular cell morphology with disrupted organization between the epithelial sheets (Fig. 6C1 and C2). These cells were separated from adjacent ameloblasts. Although elongated, the cells were plasmolysed, with reduction of the size of nuclei.

Immunofluorescence staining demonstrated that NBCe1, CFTR, and AE2 are expressed normally in the cervical loop and presecretory/secretory regions in miR-224 agomir NC-, miR-130a agomir-, miR-330 agomir-, and miR-188 agomir-, and vehicle-injected and control groups (Fig. 7D to U). miR-224 agomir treatment abrogated NBCe1 (Fig. 7A) and CFTR (Fig. 7B) in both regions but had no effect on AE2 (Fig. 7C) compared to age-matched controls, consistent with *in vitro* observations.

Notably, the immunostaining of NBCe1 and CFTR also revealed decreased expression levels in odontoblasts, and their morphology might have been affected by the miR-224 agomir treatment (Fig. 7V). This might have resulted in alterations in extracellular matrix proteins secreted from odontoblasts that potentially affect ameloblast differentiation. It has been shown that odontoblasts initiate their secretion of a collagen-based matrix under the basal lamina of PAB (17). Among all the collagen family members, collagen I (Col I) is the most abundant extracellular matrix protein in odontoblast differentiation (18). Therefore, we performed immunostaining and found unchanged expression levels of Col I in odontoblasts in miR-224 agomir-injected mice compared to miR-224 agomir NC, vehicle, and control groups (Fig. 7V).

miR-224 disrupted enamel mineralization and surface microstructure. To quantitate the structural properties of enamel, micro-CT analysis of mandibles was performed (Fig. 8). Incisor enamel lengths measured from the sagittal view did not differ among miR-224 agomir-, miR-224 agomir NC-, and vehicle-injected and control mice (Fig. 8A and C). As well-accepted observation points (19), enamel formation at the mesial bifurcate root of the first molar, the distal root of the first molar, and the mesial apex of the second molar was analyzed by micro-CT. The enamel thickness exhibited no significant difference at the mesial bifurcate root of the first molar by coronal sections (Fig. 8B [M] and

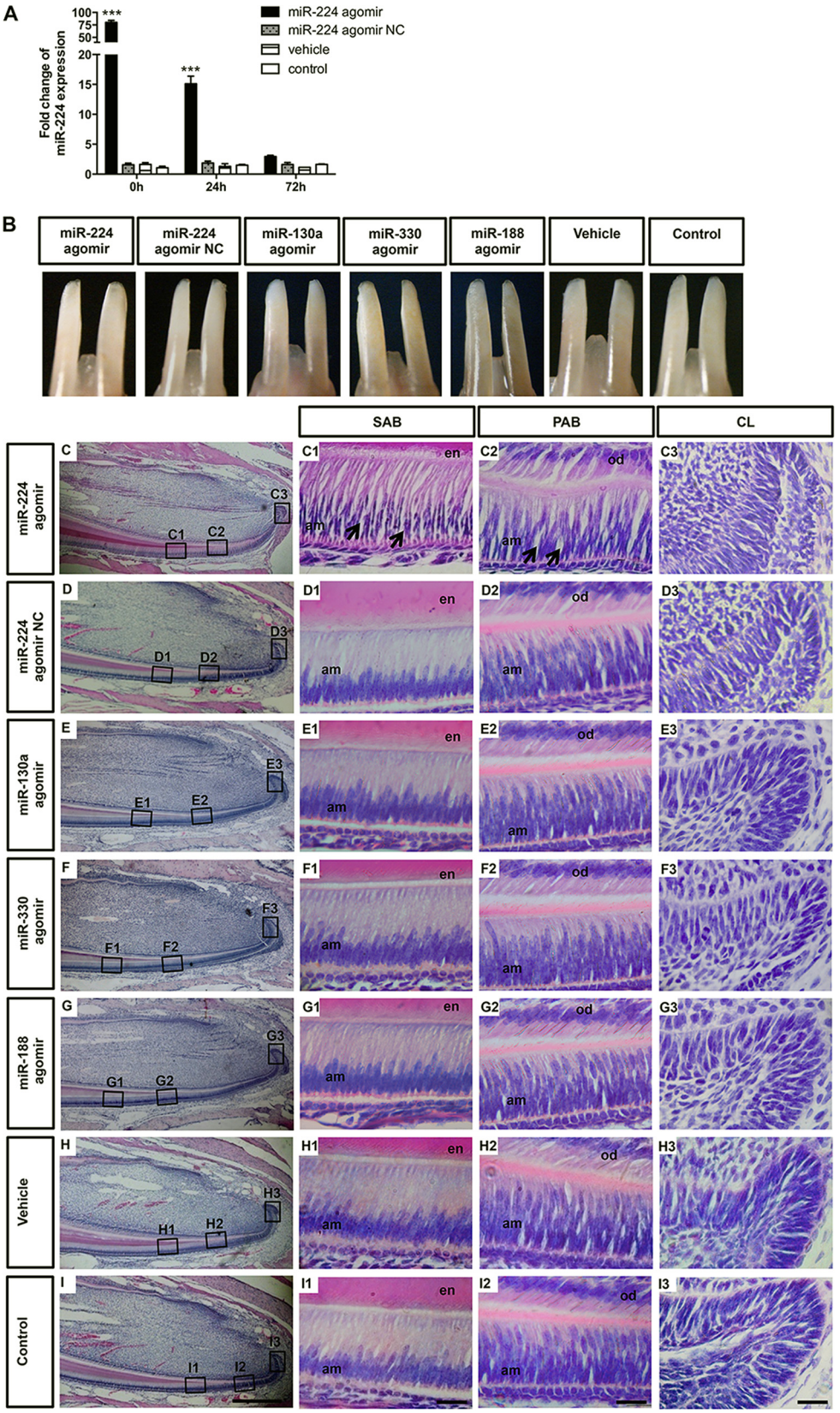

FIG 6 miR-224 disrupted ameloblast organization in developing mouse incisors. (A) Expression levels of miR-224 at 0 h, 24 h, and 72 h after a single injection of miR-224 agomir, miR-224 agomir NC, or vehicle and in control incisors. ***, $P < 0.001$ (comparison between miR-224 agomir injection and control groups; $n = 3$). The data are represented as means and SD. (B) Gross appearance of mandibular incisors of miR-224 agomir-, miR-224 agomir NC-, miR-130a agomir-, miR-330 agomir-, miR-188 agomir-, and vehicle-injected mice, as well as control mice, at P30. (C to I) H&E staining of the proximal incisor region of miR-224 agomir-injected (C), miR-224 agomir NC-injected (D), miR-130a agomir-injected (E), miR-330 agomir-injected (F), miR-188 agomir-injected (G), vehicle-injected (H), and noninjected (I) mice. Higher magnifications of SAB, PAB, and CL regions are shown to the right. Scale bars: 200 μm (C to I) and 10 μm (C1 to I3). am, ameloblasts; en, enamel; od, odontoblasts; arrows, defective ameloblasts in the miR-224 agomir-injected group.

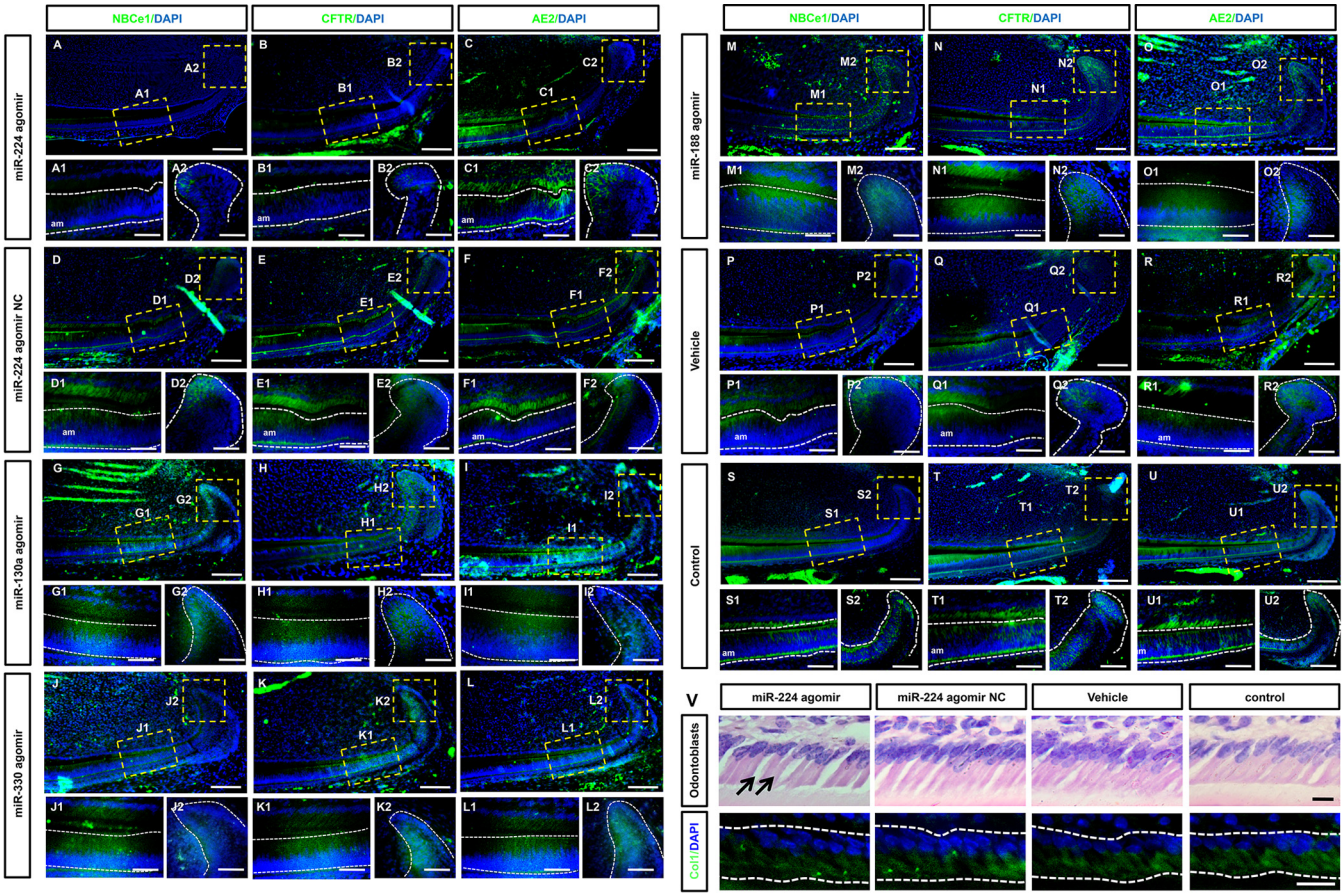

FIG 7 miR-224 affected NBCe1 and CFTR expression *in vivo*. (A to U) Immunofluorescence staining for NBCe1 (A, D, G, J, M, P, and S), CFTR (B, E, H, K, N, Q, and T), and AE2 (C, F, I, L, O, R, and U) of miR-224 agomir-injected (A to C), miR-224 agomir NC-injected (D to F), miR-130a agomir-injected (G to I), miR-330 agomir-injected (J to L), miR-188 agomir-injected (M to O), and vehicle-injected (P to R) and control (S to U) mice. (A1 to U2) High-magnification views of the yellow-boxed areas for immunofluorescence staining of NBCe1, CFTR, and AE2 in the cervical loop and presecretory/secretory stages (white dashed outlines). Lower levels of NBCe1 and CFTR were detected in miR-224 agomir-injected mice both in ameloblasts (A1 and B1) and in the cervical loop region (A2 and B2), whereas AE2 (C1 and C2) levels remained unchanged compared with multiple controls ($n = 6$). All staining is shown as merged images of NBCe1, CFTR, and AE2 in green immunofluorescence with DAPI counterstaining. Scale bars: 100 μm (A to U) and 20 μm (A1 to U2). (V) H&E staining of the odontoblasts of miR-224 agomir-, miR-224 agomir NC-, and vehicle-injected and control mice. The arrows indicate altered odontoblasts in the miR-224 agomir-injected group. Immunofluorescence staining for Col I showed unchanged expression levels after miR-224 agomir injection compared to controls. Scale bars, 20 μm.

D). No enamel could be detected at the distal root of the first molar (Fig. 8B [D]).

It has been shown that mutations in ion transporters induce developmental defects in human and murine enamel. The enamel of the incisors of NBCe1$^{-/-}$ mice appeared to be hypoplastic, with altered enamel microstructure (20, 21). CFTR knockout mice also demonstrated enamel abnormalities, with a soft and chalky white appearance. In addition, CF mouse enamel was hypomineralized and had alterations in the crystallite structures (22–24). To investigate whether miR-224 has a role in regulating enamel structure, we next analyzed details of the enamel microstructure of the incisor surface in seven experimental groups by SEM (Fig. 9). We compared the microstructures of enamel near the cutting edge (Fig. 9A to G) and cervical loop area (Fig. 9H to N). In both regions, the enamel of miR-224 agomir NC-, miR-130a agomir-, miR-330 agomir-, miR-188 agomir-, and vehicle-injected and control groups was aligned, with well-defined prism structures with the typical prism decussation structure (Fig. 9B to G and I to N). In contrast, the enamel of miR-224 agomir-treated mice, which had decreased expression of NBCe1 and CFTR, exhibited severe defects, lacking defined prism or interprism structure in any area. The crystals failed to align lengthways and lie parallel to form into rod structures, presenting abnormal crystal formation (Fig. 9A and H). In order to further confirm our observation, SEM-EDX spectra were performed to determine the enamel Ca and P content in each group, and subsequently, the Ca/P ratio was calculated. The results showed that miR-224 agomir administration significantly reduced the enamel Ca/P ratio in the incisal and cervical regions compared with multiple controls (Fig. 9O to Q). The Ca/P ratios in the miR-224 agomir NC-, miR-130a-, miR-330-, miR-188-, and vehicle-injected groups were indistinguishable compared to noninjected controls (Fig. 9O to Q), indicating that the decreased enamel Ca/P ratio was solely due to miR-224 agomir injection.

To further quantify the enamel hardness, incisors were dissected out, embedded in epoxy resin, and ground and polished for microhardness measurement. The Vickers hardness values were analyzed for each sample in both the incisal and cervical regions

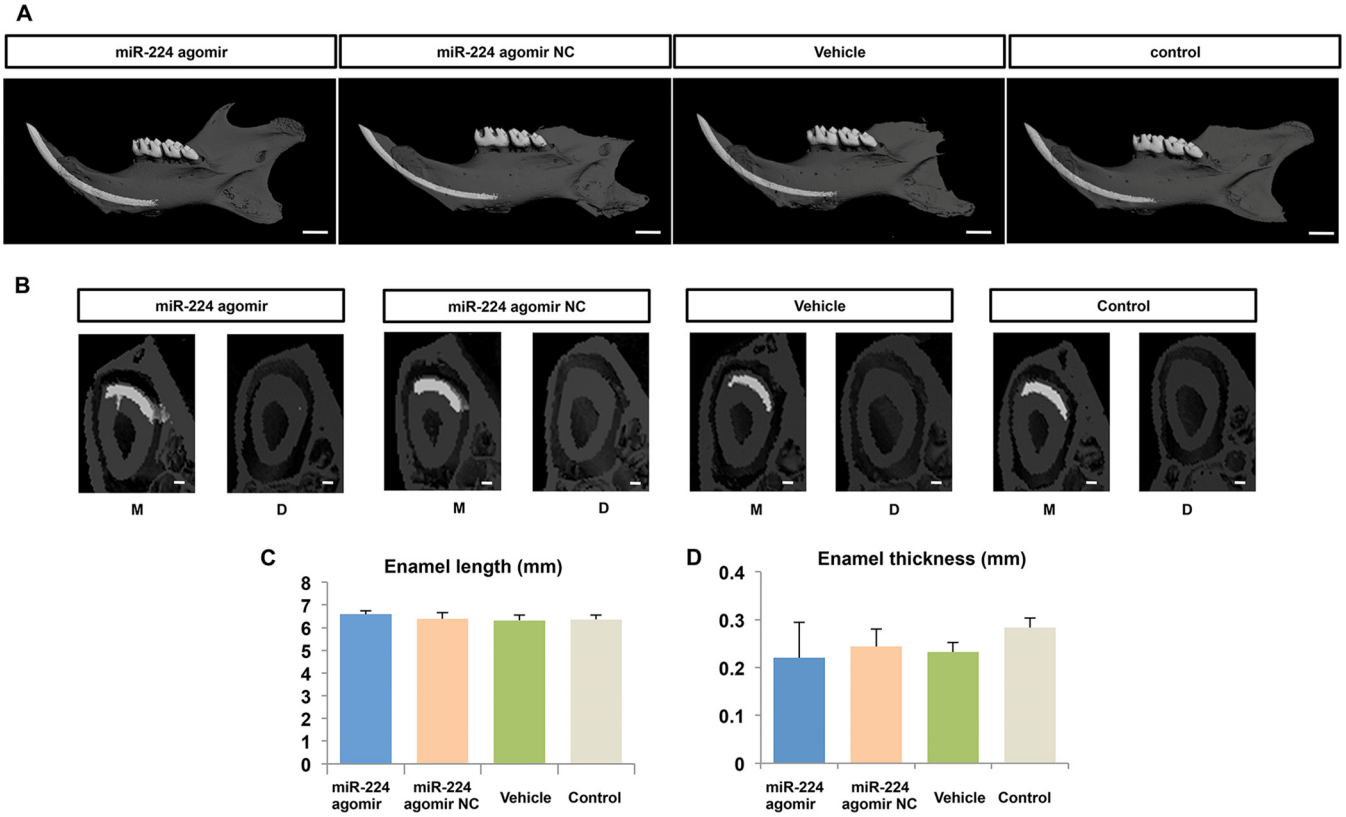

FIG 8 Micro-CT analysis. (A) Micro-CT images of hemimandibles of miR-224 agomir-, miR-224 agomir NC-, and vehicle-injected and control mice. Scale bars, 1 mm. (B) Micro-CT images of coronal sections at the mesial bifurcate root of the first molar (M) and the distal root of the first molar (D). Scale bars, 100 μm. (C) Enamel length showed no significant difference among the four groups in a midsagittal view. (D) Comparable incisor enamel thickness was identified among the four groups at the mesial bifurcate root of the first molar from coronal sections ($n = 6$). The data are represented as means and SD.

(Fig. 10A, asterisks). The enamel hardness was significantly reduced in miR-224 agomir-treated incisors in both regions. Conversely, no changes could be observed in the other groups (Fig. 10B). These observations further confirmed the specific role of miR-224 in regulating enamel mineralization *in vivo*.

DISCUSSION

Enamel is formed by terminally differentiated ameloblasts through deposition of enamel matrix (secretion), orchestration of crystal mineralization, and elimination of enamel matrix proteins (maturation). Enamel matrix proteins are secreted and serve as a scaffold guiding crystal formation (25). Hydroxyapatite crystal formation results in free-proton release [$10\ Ca^{2+} + 6\ HPO_4^{2-} + 2\ H_2O = Ca_{10}(PO_4)_6(OH)_2 + 8\ H^+$], leading to acidification of the local enamel microenvironment. The low pH in the ECM activates enamel proteinases, which degrade the matrix proteins and adjust the spatial structure, promoting further mineralization (3, 26). However, overall, the secretory-phase extracellular pH remains neutral (3). The maturation stage extracellular pH has some variability, ranging from weakly acidic to neutral and rising to higher pH values in the more advanced matured enamel (27). Therefore, an effective mechanism that can buffer protons for pH regulation is crucial for enamel mineralization (1). Ameloblasts have been proposed to play an important role in pH modulation during enamel formation by buffering amelogenin protein (3) and differential ion transporter expression during ameloblast differentiation (5, 6).

MicroRNAs posttranscriptionally modify various biological events, including tooth development, by complementarily binding to the 3′ UTRs of target mRNAs to degrade or suppress translation (7, 28–33). Specifically, miR-214 (34), miR-146a (35), miR-143/145 (36), miR-32 (28), and miR-200c/141 (28) clusters have been reported to regulate the cytodifferentiation of dental follicle cells, odontoblasts, and dental pulp cells, as well as ameloblasts. Our previous miRNA microarray analysis of different stages of developing human tooth germs yielded numerous differentially expressed miRNAs, including miR-224 (11), which is known to play a critical role in cell proliferation, migration, invasion, and antiapoptosis (37–40). To determine the spatial-temporal expression of miR-224 during enamel formation in the present study, different stages of human ameloblasts were collected *in situ* by laser capture microdissection, including PAB and SAB. The miR-224 expression level was detected in human dental epithelial cells and significantly decreased as ameloblasts differentiated. We also observed a marked decrease of miR-224 expression under an acidic environment (pH 6.2) in cultured human ameloblast lineage cells.

Prediction tools indicated that the target genes of miR-224 include genes encoding a set of crucial ion transporters required for the development of normal enamel, including *SLC4A4* and *CFTR* (5, 6, 41). NBCe1 (encoded by *SLC4A4*), AE2 (encoded by *SLC4A2*), and CFTR (encoded by *CFTR*) have been proposed to compose a buffering system during ameloblast differentiation and

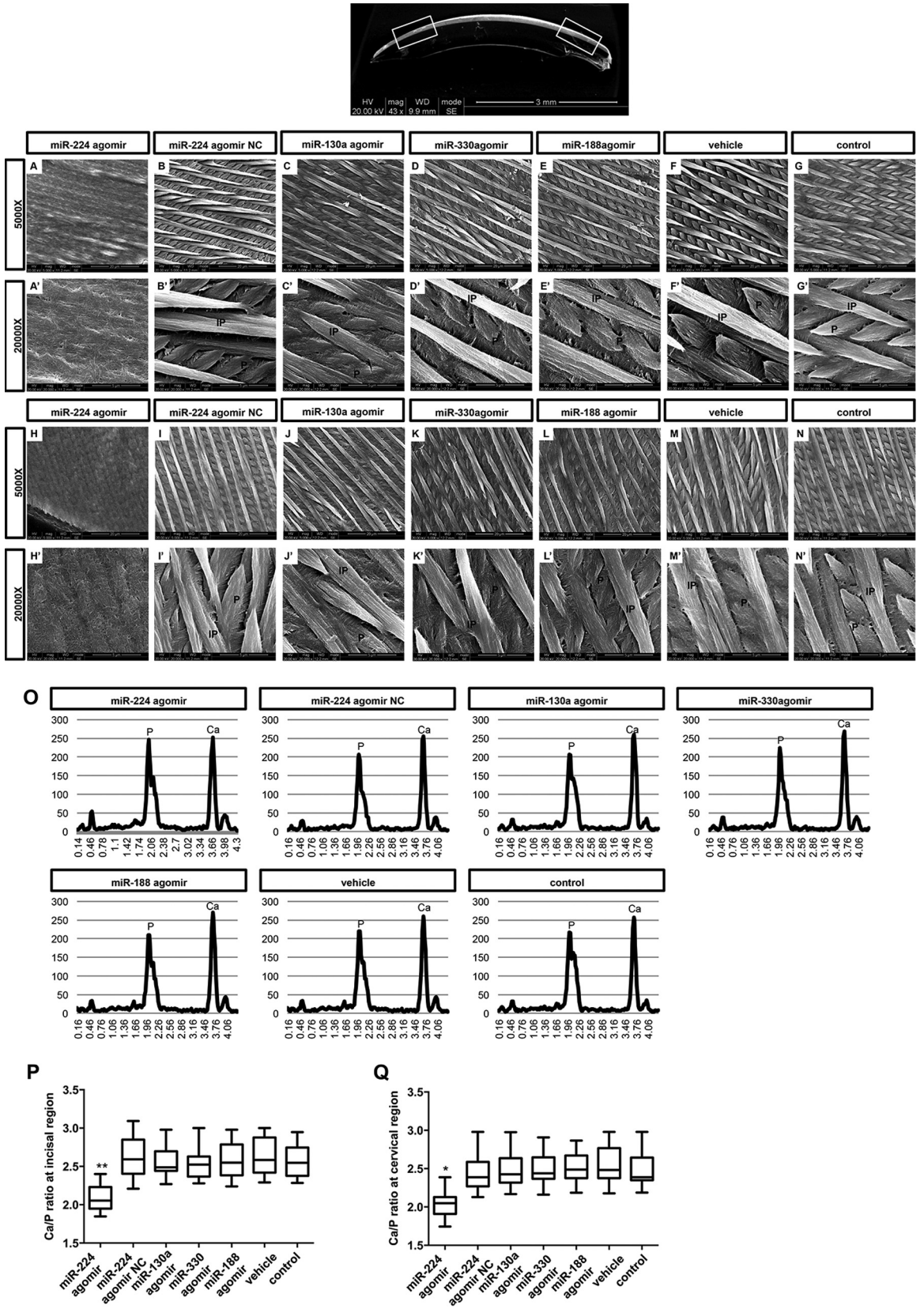

FIG 9 SEM and SEM-EDX spectroscopy of incisors. Incisors were stripped from lower jaws and ground to check microstructure near the cusp (A to G and A′ to G′) and cervical loop area (H to N and H′ to N′). miR-224 agomir-treated mice showed severe defects, with no defined prism or interprism in both the incisal and cervical regions (A, A′, H, and H′), while miR-224 agomir NC-injected (B, B′, I, and I′), miR-130a agomir-injected (C, C′, J, and J′), miR-330 agomir-injected (D, D′, K, and K′), miR-188 agomir-injected (E, E′, L, and L′), and vehicle-injected (F, F′, M, and M′) and control (G, G′, N, and N′) groups were aligned, with well-defined prism structures with the typical prism decussation structure. P, prism; IP, interprism. Scale bars: 20 μm (A to N) and 5 μm (A′ to N′). (O) EDX spectra of seven experimental groups. (P and Q) The Ca/P ratio was significantly decreased in the incisal (P) and cervical (Q) regions of the miR-224 agomir-injected group compared to multiple controls. *, $P < 0.05$; **, $P < 0.01$; $n = 5$ or 6. The whiskers indicate the data range, and the horizontal lines in the boxes represent the averages.

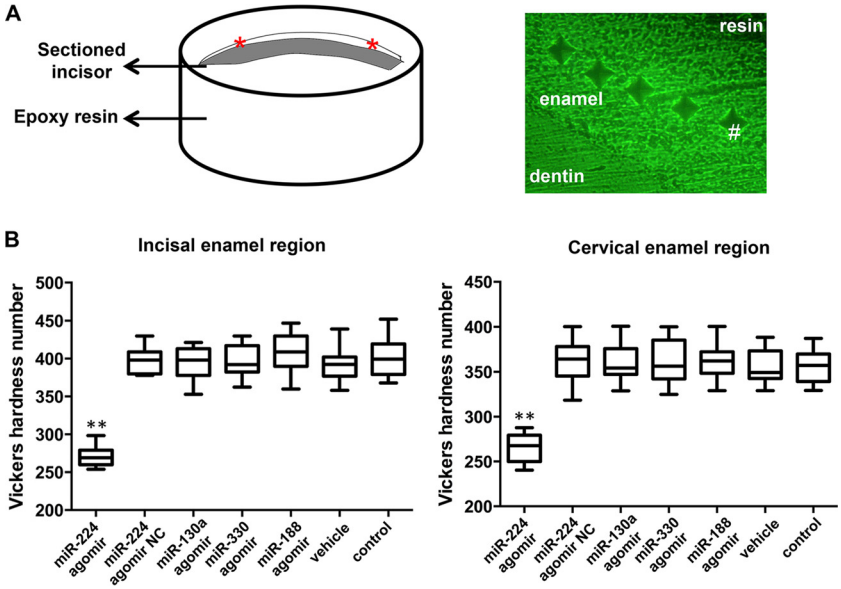

FIG 10 Quantification of enamel hardness. (A) Schematic graph of sample preparation for Vickers hardness assessment and 10 indentations in both incisal and cervical regions of the enamel layer obtained per incisor. The asterisks indicate the measured region, and the pound sign indicates the indentations. (B) Enamel hardness was significantly and specifically reduced after miR-224 agomir injection in the incisal and cervical regions compared to multiple groups. **, $P < 0.01$; $n = 4$ to 6. The whiskers indicate the data range, and the horizontal lines in the boxes represent the averages of microhardness values.

enamel mineralization (5, 6). These transporters control the uptake and efflux of many critical ions or substrates during amelogenesis and have been determined to result in enamel abnormalities if mutated. Mutations in *SLC4A4* result in pigmentation differences and a propensity to fracture (21, 42–46). Patients with proximal renal tubular acidosis (pRTA) caused by mutations in *SLC4A4* also exhibit dental abnormalities (5, 42). People with CF due to mutations in *CFTR* may have dental enamel defects (47–51). *Cftr* knockout mice confirmed the presence of this chloride channel in ameloblasts and its pivotal role in modulating amelogenesis by affecting pH (23, 52). Located on the apical or basolateral membrane of polarized ameloblasts, NBCe1 and AE2 regulate intra- and extracellular pH by mediating the electrogenic transport of Na^+ and bases (HCO_3^- and CO_3^{2-}) (5). More recently, NBCe1 has been found in mouse dental epithelium and might be engaged in neutralizing protons released during crystal formation in the enamel space, thus regulating pH (53). In the current study, *SLC4A4* and *CFTR* expression levels were significantly increased during human ameloblast differentiation, inversely linearly correlating with miR-224 expression. In accordance with previous studies showing that *SLC4A4* mRNA expression is pH dependent (5, 54, 55), we found that *in vitro* acidification treatment in cultured human ALCs resulted in significant upregulation of both *SLC4A4* and *CFTR* mRNA expression levels, again inversely correlating with miR-224 expression. A dual-luciferase assay revealed that miR-224 binds to the 3′ UTRs of *SLC4A4* and *CFTR* directly and thus posttranscriptionally regulates these genes. Both the mRNA and protein levels of *SLC4A4* and *CFTR* were affected by transfection with miR-224 oligonucleotides in cultured human ALCs and OEs. Other selected miRNAs (i.e., miR-130a, miR330, and miR-188) had no effect on *SLC4A4* and *CFTR* expression levels. Thus, we propose that miR-224 specifically affects *SLC4A4* and *CFTR* directly in human ALCs and OEs and might play a pivotal role in buffering pH values and modulating enamel mineralization.

We used local injection of modified oligonucleotides to determine the *in vivo* effects of miR-224, as there is no genetic mouse model currently available. The continuously growing incisors in mice provide an excellent model to examine the regulation of enamel development, since they contain different stages of ameloblasts and the features of each phase are well characterized. This allows us to determine the effect of miR-224 on ameloblast differentiation postnatally. MicroRNA agomir is a chemically modified oligonucleotide widely applied in microRNA investigation (56, 57). Injection of miR-224 agomir resulted in abnormal ameloblast morphology and decreased target ion transporter expression. NBCe1 and CFTR immunostaining showed reduced signal in miR-224 agomir-treated incisors, whereas AE2 remained unchanged, consistent with *in vitro* results. Micro-CT analysis revealed no statistical difference in the incisor enamel length and thickness among miR-224 agomir-, miR-224 agomir NC-, and vehicle-injected mice and noninjected control mice. Moreover, miR-224 had no impact on the expression of major enamel proteins. AMLX and AMBN are important in the extracellular matrix of enamel; however, they are not necessarily key factors in the mineralization of the enamel. For example, in some cases of amelogenesis imperfecta (AI), the matrix secretion of ameloblasts could be normal, but with hypomineralized enamel. Although the ameloblasts might maintain normal secretory function, enamel with miR-224 agomir treatment showed severely disturbed organization of the prism parallel structures and deficient crystal growth in the interprisms. Moreover, the enamel microhardness, as well as the Ca/P ratio, was markedly decreased after miR-224 agomir injection, whereas injection of other miRNA agomirs produced rather normal enamel properties, indicating the specificity of miR-224 function in enamel mineralization. The dramatic defects in crystal formation shown by SEM were not reflected in obvious changes in enamel color, transparency, and relative intensity observed by stereomicroscope or micro-CT. Possible explanations for the inconspicuous gross phenotype may be as follows.

The mouse incisor enamel encompasses four layers, a thin, inner, prism-free layer; an inner enamel layer with prism decussation; an outer enamel layer with parallel prisms; and a thin, superficial, prism-free layer (58). Changes in the crystal microstructure might not be detectable by eye or with a stereomicroscope. A recent study using *in vivo* transfection of anti-miR214 also showed no obvious enamel morphological changes observed with a stereomicroscope, but further SEM analysis indicated alterations in the prism decussation structure (59).

Several studies proposed scenarios regarding the effect of changes in pH conditions on the growth of apatite crystals (27). The defects in the microarchitecture of the enamel surface in miR-224 agomir-treated mice may be due to abnormalities in ion transporters on the membranes of ameloblasts, resulting in subsequent changes in the pH in the extracellular buffering microenvironment during enamel mineralization. It has been suggested that the most critical property of hydroxyapatite is its carbonate substitution, which might control apatite crystal size. The potential changes in the buffering system by decreased NBCe1 and CFTR after miR-224 agomir injection might have a direct impact on the physical and chemical properties of apatite and ultimately lead to changes in the crystal structure and microhardness. The significant defects in enamel microstructure and reduced microhardness of miR-224 agomir-treated mice resembled the hypomineralized enamel phenotype that is associated with amelogenesis imperfecta.

Histological analysis suggested alterations of adjacent odontoblasts to some extent. We suspected that the changes in the extracellular matrix secreted from dentin when predentin starts to form may have some effect on the enamel microstructure. Therefore, we evaluated the expression of Col I as a major substance in the dentin meshwork and found unchanged expression levels after miR-224 agomir injection compared to multiple controls. Over the past several years, genetic studies in patients with osteogenesis imperfecta, dentinogenesis imperfecta, and dentin dysplasia caused by defined mutations in COL1A1, COL1A2, and DSPP exhibited rather normal ameloblast differentiation and enamel formation (15), suggesting the odontoblast defect found in the present study might not be directly responsible for the alterations in ameloblasts and that the regulation by miR-224 of dentin formation needs to be further explored.

Enamel mineralization is accomplished before tooth eruption and is affected by several internal and external factors aside from pH. Dental fluorosis is caused by excessive intake of fluoride during tooth development and results in enamel hypomineralization, characterized by white spots, brown stains, pitting, or mottling of the enamel. These enamel phenotypes are quite similar to those seen with mutation or deletion of cotransporters, chloride channels, and functional exchangers in ameloblasts (5, 23, 24). It is thus speculated that these genes may be modulated by fluoride treatment. To imitate dental fluorosis, the cell culture media were supplemented with fluoride, as described previously (6). Fluoride exposure in cultured human ALCs had no effect on ion channels (*SLC4A4*, *CFTR*, and *SLC4A2*) or miR-224, which is in line with the previous studies indicating that the effect of fluoride on increasing expression of SLC4A4 *in vivo* is the result of fluoride-induced matrix acidification, rather than a direct effect on mRNA expression. Further *in vivo* studies to measure miR-224 in ameloblasts from fluorosed mouse incisors would further confirm this proposed function of fluoride in acidifying the enamel matrix during enamel biomineralization.

Collectively, these data indicate that miR-224 specifically regulates the ion transporters *SLC4A4* and *CFTR* and leads to subsequent fine tuning of enamel mineralization during amelogenesis, with minimal effect on ameloblast secretion. By direct targeting, miR-224 in ameloblasts serves to maintain the desired expression of NBCe1 and CFTR and thus to maintain pH homeostasis, consequently contributing to enamel mineralization.

ACKNOWLEDGMENTS

This study was supported by NSFC grants 81371136 and JCPT2011-9 to Xuedong Zhou and NSFC grants 81470711 and 81200760 to L.Z.

We thank Joseph Modonza for the contribution of Fig. 1A.

Author contributions were as follows: study design, L.Z. and Y.F.; study conduct, Y.F., Y.Z., and M.W.; data collection, Y.Z., Xin Zhou, and B.G.; data analysis, B.G., Xuedong Zhou, and X.X.; data interpretation, L.Z., Y.F., J.S., and F.S.; drafting the manuscript, L.Z. and Y.F.; revising the manuscript content, L.Z., L.C., and J.C.; approving the final version of the manuscript, L.Z., J.C., X.X., and Xuedong Zhou. L.Z. takes responsibility for the integrity of the data analysis.

REFERENCES

1. **Smith CE.** 1998. Cellular and chemical events during enamel maturation. Crit Rev Oral Biol Med **9:**128–161. http://dx.doi.org/10.1177/10454411980090020101.
2. **Bartlett JD.** 2013. Dental enamel development: proteinases and their enamel matrix substrates. ISRN Dent **2013:**684607. http://dx.doi.org/10.1155/2013/684607.
3. **Simmer JP, Fincham AG.** 1995. Molecular mechanisms of dental enamel formation. Crit Rev Oral Biol Med **6:**84–108. http://dx.doi.org/10.1177/10454411950060020701.
4. **Sasaki T, Tadokoro K, Yanagisawa T, Higashi S, Garant PR.** 1988. H+-K+-ATPase activity in the rat incisor enamel organ during enamel formation. Anat Rec **221:**823–833. http://dx.doi.org/10.1002/ar.1092210406.
5. **Paine ML, Snead ML, Wang HJ, Abuladze N, Pushkin A, Liu W, Kao LY, Wall SM, Kim YH, Kurtz I.** 2008. Role of NBCe1 and AE2 in secretory ameloblasts. J Dent Res **87:**391–395. http://dx.doi.org/10.1177/154405910808700415.
6. **Zheng L, Zhang Y, He P, Kim J, Schneider R, Bronckers AL, Lyaruu DM, DenBesten PK.** 2011. NBCe1 in mouse and human ameloblasts may be indirectly regulated by fluoride. J Dent Res **90:**782–787. http://dx.doi.org/10.1177/0022034511398273.
7. **Bartel DP.** 2004. MicroRNAs: genomics, biogenesis, mechanism, and function. Cell **116:**281–297. http://dx.doi.org/10.1016/S0092-8674(04)00045-5.
8. **Lamouille S, Subramanyam D, Blelloch R, Derynck R.** 2013. Regulation of epithelial-mesenchymal and mesenchymal-epithelial transitions by microRNAs. Curr Opin Cell Biol **25:**200–207. http://dx.doi.org/10.1016/j.ceb.2013.01.008.
9. **Ramachandran S, Karp PH, Jiang P, Ostedgaard LS, Walz AE, Fisher JT, Keshavjee S, Lennox KA, Jacobi AM, Rose SD, Behlke MA, Welsh MJ, Xing Y, McCray PB, Jr.** 2012. A microRNA network regulates expression and biosynthesis of wild-type and DeltaF508 mutant cystic fibrosis transmembrane conductance regulator. Proc Natl Acad Sci U S A **109:**13362–13367. http://dx.doi.org/10.1073/pnas.1210906109.
10. **Banales JM, Saez E, Uriz M, Sarvide S, Urribarri AD, Splinter P, Tietz Bogert PS, Bujanda L, Prieto J, Medina JF, LaRusso NF.** 2012. Up-regulation of microRNA 506 leads to decreased Cl-/HCO3- anion exchanger 2 expression in biliary epithelium of patients with primary biliary cirrhosis. Hepatology **56:**687–697. http://dx.doi.org/10.1002/hep.25691.
11. **Wan M, Gao B, Sun F, Tang Y, Ye L, Fan Y, Klein OD, Zhou X, Zheng L.** 2012. MicroRNA miR-34a regulates cytodifferentiation and targets multi-signaling pathways in human dental papilla cells. PLoS One **7:**e50090. http://dx.doi.org/10.1371/journal.pone.0050090.
12. **Zheng LW, Linthicum L, DenBesten PK, Zhang Y.** 2013. The similarity between human embryonic stem cell-derived epithelial cells and ameloblast-lineage cells. Int J Oral Sci **5:**1–6. http://dx.doi.org/10.1038/ijos.2013.14.
13. **Staszel T, Zapala B, Polus A, Sadakierska-Chudy A, Kiec-Wilk B, Stepien E, Wybranska I, Chojnacka M, Dembinska-Kiec A.** 2011. Role

of microRNAs in endothelial cell pathophysiology. Pol Arch Med Wewn **121:**361–366.
14. **Zhang Q, Kandic I, Kutryk MJ.** 2011. Dysregulation of angiogenesis-related microRNAs in endothelial progenitor cells from patients with coronary artery disease. Biochem Biophys Res Commun **405:**42–46. http://dx.doi.org/10.1016/j.bbrc.2010.12.119.
15. **Hu JC, Chun YH, Al Hazzazzi T, Simmer JP.** 2007. Enamel formation and amelogenesis imperfecta. Cells Tissues Organs **186:**78–85. http://dx.doi.org/10.1159/000102683.
16. **Richards A.** 1990. Nature and mechanisms of dental fluorosis in animals. J Dent Res **69:**701–705, 721.
17. **Hu JC, Simmer JP.** 2007. Developmental biology and genetics of dental malformations. Orthod Craniofac Res **10:**45–52. http://dx.doi.org/10.1111/j.1601-6343.2007.00384.x.
18. **Yoshizaki K, Yamada Y.** 2013. Gene evolution and functions of extracellular matrix proteins in teeth. Orthod Waves **72:**1–10. http://dx.doi.org/10.1016/j.odw.2013.01.040.
19. **Smith CE, Nanci A.** 1989. A method for sampling the stages of amelogenesis on mandibular rat incisors using the molars as a reference for dissection. Anat Rec **225:**257–266. http://dx.doi.org/10.1002/ar.1092250312.
20. **Lacruz RS, Nanci A, White SN, Wen X, Wang H, Zalzal SF, Luong VQ, Schuetter VL, Conti PS, Kurtz I, Paine ML.** 2010. The sodium bicarbonate cotransporter (NBCe1) is essential for normal development of mouse dentition. J Biol Chem **285:**24432–24438. http://dx.doi.org/10.1074/jbc.M110.115188.
21. **Gawenis LR, Bradford EM, Prasad V, Lorenz JN, Simpson JE, Clarke LL, Woo AL, Grisham C, Sanford LP, Doetschman T, Miller ML, Shull GE.** 2007. Colonic anion secretory defects and metabolic acidosis in mice lacking the NBC1 Na+/HCO3- cotransporter. J Biol Chem **282:**9042–9052. http://dx.doi.org/10.1074/jbc.M607041200.
22. **Snouwaert JN, Brigman KK, Latour AM, Malouf NN, Boucher RC, Smithies O, Koller BH.** 1992. An animal model for cystic fibrosis made by gene targeting. Science **257:**1083–1088. http://dx.doi.org/10.1126/science.257.5073.1083.
23. **Wright JT, Kiefer CL, Hall KI, Grubb BR.** 1996. Abnormal enamel development in a cystic fibrosis transgenic mouse model. J Dent Res **75:**966–973. http://dx.doi.org/10.1177/00220345960750041101.
24. **Wright JT, Hall KI, Grubb BR.** 1996. Enamel mineral composition of normal and cystic fibrosis transgenic mice. Adv Dent Res **10:**270–274, 275. http://dx.doi.org/10.1177/08959374960100022501.
25. **Beniash E, Simmer JP, Margolis HC.** 2005. The effect of recombinant mouse amelogenins on the formation and organization of hydroxyapatite crystals in vitro. J Struct Biol **149:**182–190. http://dx.doi.org/10.1016/j.jsb.2004.11.001.
26. **Smith CE, Issid M, Margolis HC, Moreno EC.** 1996. Developmental changes in the pH of enamel fluid and its effects on matrix-resident proteinases. Adv Dent Res **10:**159–169. http://dx.doi.org/10.1177/08959374960100020701.
27. **Lacruz RS, Nanci A, Kurtz I, Wright JT, Paine ML.** 2010. Regulation of pH during amelogenesis. Calc Tissue Int **86:**91–103. http://dx.doi.org/10.1007/s00223-009-9326-7.
28. **Cao H, Wang J, Li X, Florez S, Huang Z, Venugopalan SR, Elangovan S, Skobe Z, Margolis HC, Martin JF, Amendt BA.** 2010. MicroRNAs play a critical role in tooth development. J Dent Res **89:**779–784. http://dx.doi.org/10.1177/0022034510369304.
29. **Tang G, Tang X, Mendu V, Tang X, Jia X, Chen QJ, He L.** 2008. The art of microRNA: various strategies leading to gene silencing via an ancient pathway. Biochim Biophys Acta **1779:**655–662. http://dx.doi.org/10.1016/j.bbagrm.2008.06.006.
30. **Michon F, Tummers M, Kyyronen M, Frilander MJ, Thesleff I.** 2010. Tooth morphogenesis and ameloblast differentiation are regulated by micro-RNAs. Dev Biol **340:**355–368. http://dx.doi.org/10.1016/j.ydbio.2010.01.019.
31. **Liu J, Zheng M, Tang YL, Liang XH, Yang Q.** 2011. MicroRNAs, an active and versatile group in cancers. Int J Oral Sci **3:**165–175. http://dx.doi.org/10.4248/IJOS11063.
32. **Gao B, Zheng L.** 2013. microRNA expression in rat apical periodontitis bone lesion. Bone Res **1:**170–185. http://dx.doi.org/10.4248/BR201302006.
33. **Llobet-Navas D, Rodriguez-Barrueco R, de la Iglesia-Vicente J, Olivan M, Castro V, Saucedo-Cuevas L, Marshall N, Putcha P, Castillo-Martin M, Bardot E, Ezhkova E, Iavarone A, Cordon-Cardo C, Silva JM.** 2014. The microRNA 424/503 cluster reduces CDC25A expression during cell cycle arrest imposed by transforming growth factor beta in mammary epithelial cells. Mol Cell Biol **34:**4216–4231. http://dx.doi.org/10.1128/MCB.00611-14.
34. **Khan QE, Sehic A, Khuu C, Risnes S, Osmundsen H.** 2013. Expression of Clu and Tgfb1 during murine tooth development: effects of in-vivo transfection with anti-miR-214. Eur J Oral Sci **121:**303–312. http://dx.doi.org/10.1111/eos.12056.
35. **Chen P, Wei D, Xie B, Ni J, Xuan D, Zhang J.** 2014. Effect and possible mechanism of network between microRNAs and RUNX2 gene on human dental follicle cells. J Cell Biochem **115:**340–348. http://dx.doi.org/10.1002/jcb.24668.
36. **Liu H, Lin H, Zhang L, Sun Q, Yuan G, Zhang L, Chen S, Chen Z.** 2013. miR-145 and miR-143 regulate odontoblast differentiation through targeting Klf4 and Osx genes in a feedback loop. J Biol Chem **288:**9261–9271. http://dx.doi.org/10.1074/jbc.M112.433730.
37. **Wang Y, Ren J, Gao Y, Ma JZ, Toh HC, Chow P, Chung AY, Ooi LL, Lee CG.** 2013. MicroRNA-224 targets SMAD family member 4 to promote cell proliferation and negatively influence patient survival. PLoS One **8:**e68744. http://dx.doi.org/10.1371/journal.pone.0068744.
38. **Yao G, Liang M, Liang N, Yin M, Lu M, Lian J, Wang Y, Sun F.** 2014. MicroRNA-224 is involved in the regulation of mouse cumulus expansion by targeting Ptx3. Mol Cell Endocrinol **382:**244–253. http://dx.doi.org/10.1016/j.mce.2013.10.014.
39. **Zhang Y, Takahashi S, Tasaka A, Yoshima T, Ochi H, Chayama K.** 2013. Involvement of microRNA-224 in cell proliferation, migration, invasion, and anti-apoptosis in hepatocellular carcinoma. J Gastroenterol Hepatol **28:**565–575. http://dx.doi.org/10.1111/j.1440-1746.2012.07271.x.
40. **Wang P, Zhao L, Liu J, Weir MD, Zhou X, Xu HHK.** 2014. Bone tissue engineering via nanostructured calcium phosphate biomaterials and stem cells. Bone Res **2:**14017. http://dx.doi.org/10.1038/boneres.2014.17.
41. **Urzua B, Ortega-Pinto A, Morales-Bozo I, Rojas-Alcayaga G, Cifuentes V.** 2011. Defining a new candidate gene for amelogenesis imperfecta: from molecular genetics to biochemistry. Biochem Genet **49:**104–121. http://dx.doi.org/10.1007/s10528-010-9392-6.
42. **Dinour D, Chang MH, Satoh J, Smith BL, Angle N, Knecht A, Serban I, Holtzman EJ, Romero MF.** 2004. A novel missense mutation in the sodium bicarbonate cotransporter (NBCe1/SLC4A4) causes proximal tubular acidosis and glaucoma through ion transport defects. J Biol Chem **279:**52238–52246. http://dx.doi.org/10.1074/jbc.M406591200.
43. **Inatomi J, Horita S, Braverman N, Sekine T, Yamada H, Suzuki Y, Kawahara K, Moriyama N, Kudo A, Kawakami H, Shimadzu M, Endou H, Fujita T, Seki G, Igarashi T.** 2004. Mutational and functional analysis of SLC4A4 in a patient with proximal renal tubular acidosis. Pflugers Arch **448:**438–444.
44. **Baubec T, Schubeler D.** 2014. Genomic patterns and context specific interpretation of DNA methylation. Curr Opin Genet Dev **25:**85–92. http://dx.doi.org/10.1016/j.gde.2013.11.015.
45. **Brommage R, Liu J, Hansen G.** 2014. High-throughput screening of mouse gene knockouts identifies established and novel skeletal phenotypes. Bone Res **2:**14034. http://dx.doi.org/10.1038/boneres.2014.34.
46. **Su N, Jin M, Chen L.** 2014. Role of FGF/FGFR signaling in skeletal development and homeostasis: learning from mouse models. Bone Res **2:**14003. http://dx.doi.org/10.1038/boneres.2014.3.
47. **Primosch RE.** 1980. Tetracycline discoloration, enamel defects, and dental caries in patients with cystic fibrosis. Oral Surg Oral Med Oral Pathol **50:**301–308. http://dx.doi.org/10.1016/0030-4220(80)90411-9.
48. **Azevedo TD, Feijo GC, Bezerra AC.** 2006. Presence of developmental defects of enamel in cystic fibrosis patients. J Dent Child **73:**159–163.
49. **Cua FT.** 1991. Calcium and phosphorous in teeth from children with and without cystic fibrosis. Biol Trace Elem Res **30:**277–289. http://dx.doi.org/10.1007/BF02991422.
50. **Ferrazzano GF, Sangianantoni G, Cantile T, Amato I, Orlando S, Ingenito A.** 2012. Dental enamel defects in Italian children with cystic fibrosis: an observational study. Community Dent Health **29:**106–109.
51. **Lacruz RS, Smith CE, Bringas P, Jr, Chen YB, Smith SM, Snead ML, Kurtz I, Hacia JG, Hubbard MJ, Paine ML.** 2012. Identification of novel candidate genes involved in mineralization of dental enamel by genome-wide transcript profiling. J Cell Physiol **227:**2264–2275. http://dx.doi.org/10.1002/jcp.22965.
52. **Arquitt CK, Boyd C, Wright JT.** 2002. Cystic fibrosis transmembrane regulator gene (CFTR) is associated with abnormal enamel formation. J Dent Res **81:**492–496. http://dx.doi.org/10.1177/154405910208100712.
53. **Jalali R, Guo J, Zandieh-Doulabi B, Bervoets TJ, Paine ML, Boron WF, Parker MD, Bijvelds MJ, Medina JF, DenBesten PK, Bronckers AL.**

2014. NBCe1 (SLC4A4) a potential pH regulator in enamel organ cells during enamel development in the mouse. Cell Tissue Res **358:**433–442. http://dx.doi.org/10.1007/s00441-014-1935-4.

54. **Smith CE, Chong DL, Bartlett JD, Margolis HC.** 2005. Mineral acquisition rates in developing enamel on maxillary and mandibular incisors of rats and mice: implications to extracellular acid loading as apatite crystals mature. J Bone Miner Res **20:**240–249.
55. **Josephsen K, Takano Y, Frische S, Praetorius J, Nielsen S, Aoba T, Fejerskov O.** 2010. Ion transporters in secretory and cyclically modulating ameloblasts: a new hypothesis for cellular control of preeruptive enamel maturation. Am J Physiol Cell Physiol **299:**C1299–C1307. http://dx.doi.org/10.1152/ajpcell.00218.2010.
56. **Yang M, Wei Y, Jiang F, Wang Y, Guo X, He J, Kang L.** 2014. MicroRNA-133 inhibits behavioral aggregation by controlling dopamine synthesis in locusts. PLoS Genet **10:**e1004206. http://dx.doi.org/10.1371/journal.pgen.1004206.
57. **Zhu J, Chen T, Yang L, Li Z, Wong MM, Zheng X, Pan X, Zhang L, Yan H.** 2012. Regulation of microRNA-155 in atherosclerotic inflammatory responses by targeting MAP3K10. PLoS One **7:**e46551. http://dx.doi.org/10.1371/journal.pone.0046551.
58. **Sehic A, Peterkova R, Lesot H, Risnes S.** 2009. Distribution and structure of the initial dental enamel formed in incisors of young wild-type and Tabby mice. Eur J Oral Sci **117:**644–654. http://dx.doi.org/10.1111/j.1600-0722.2009.00676.x.
59. **Sehic A, Risnes S, Khuu C, Khan QE, Osmundsen H.** 2011. Effects of in vivo transfection with anti-miR-214 on gene expression in murine molar tooth germ. Physiol Genomics **43:**488–498. http://dx.doi.org/10.1152/physiolgenomics.00248.2010.